# Hydrodynamic Model Fitting for Wave Energy Applications Using Moment-Matching: A Case Study

*Yerai Peña-Sanchez, Nicolás Faedo and John V. Ringwood*
Centre for Ocean Energy Research, Maynooth University, Maynooth, Ireland

## ABSTRACT

Several methods have been developed to identify a parametric model that represents the radiation force convolution term in Cummins' equation. The reason behind such an approximation is twofold: obtaining a model with less computational (effort) requirements, and easing model-based control design procedures. In this paper, a case study on the parametric approximation of such a convolution term using frequency-domain data is considered, based on recent advances in model order reduction by moment-matching. Both the force-to-motion and radiation impulse response dynamics are considered. The advantages of a moment-based strategy are discussed, while providing a comparison with well-known existing methods.

KEY WORDS: Radiation forces; Parametric form; Model order reduction; Frequency domain identification; Moment-matching

## INTRODUCTION

Several methods have been developed to obtain the hydrodynamic coefficients for the mathematical models of floating bodies, such as Boundary Element Methods (BEMs), Computational Fluid Dynamics (CFD) or Smoothed-Particle Hydrodynamics (SPH). The speed with which the hydrodynamic coefficients are computed using BEM makes it a common choice to compute such parameters for a floating body (Penalba et al., 2017a). To compute the hydrodynamic coefficients of a Wave Energy Converter (WEC), the most widely used BEMs are the open-source software NEMOH (Babarit and Delhommeau, 2015) and the commercially available software WAMIT (Newman and Lee, 2002). One of the handicaps of BEMs is that the coefficients are given in the frequency-domain and, therefore, only the steady-state motion of the WEC is characterised. Since the motion of the free surface in a realistic sea state rarely reaches steady-state conditions, a time-domain representation gives a more comprehensive description, which is useful in several applications. The dynamics of a WEC can be expressed in the time-domain using the well-known Cummins' equation (Cummins, 1962). The relationship between the hydrodynamic frequency-domain data obtained by BEMs and Cummins' equation is given in (Ogilvie, 1964), and recalled in this study in the section "WEC equations of motion". The resulting time-domain representation includes a convolution term to characterise the fluid memory effects associated with the radiation forces acting on the device.

The main disadvantages of such a convolution term is that it is both computationally expensive and inconvenient for any model-based control design procedures, which are usually based on state-space representations of the system under analysis. In fact, the vast majority of the optimal control techniques which attempt to maximise the absorbed energy of the WEC, found in the literature, require a state-space approximation of the convolution term (Faedo et al., 2017a).

Several methods to approximate the radiation convolution term using a time-invariant state-space representation can be found in the literature, as discussed in, for example, (Faedo et al., 2017b). One of the most popular methods, referred to in this paper as the NTNU method (Pérez and Fossen, 2008), consists of finding a state-space representation based on the frequency response of the radiation force system, which can be computed using the hydrodynamic frequency-domain data obtained from BEM solvers. Another widely used strategy is Prony's method (Duclos et al., 2001, De Prony, 1795), which finds a state-space representation by first approximating the radiation force impulse response by a weighted sum of complex exponentials. Such an impulse response is usually generated from the frequency-domain data obtained by BEM solvers, due to the computational requirements of time-domain solvers, but time-domain solvers are also used (Achil3D).

Overall, an ideal parametric approximation of a WEC model should represent as closely as possible the target device dynamics over a given frequency range, which should be wide enough to include all the relevant (from an energetic perspective) input frequencies. In fact, there are some frequencies that have a strong impact on the system dynamics such as, for example, the resonant frequency of the device. Therefore, an important objective for any approximation would be to match the behaviour of the WEC on those key frequencies. Another feature of an ideal identification technique is that the error of the approximation should always decrease while increasing the order of the approximated model, which is not always the case, as already reported for several strategies.

Considering the characteristics that an ideal parametric approximation should satisfy, Faedo et al. (2017b) introduces an approximation technique based on recent advances on model order reduction by moment-matching. Moment-matching methods are based on the idea of interpolating a certain number of points on the complex plane called *moments*. Such moments have a direct relationship with the frequency-response of

the dynamical system under analysis. In fact, the transfer function of the reduced order model obtained by moment-matching exactly matches the behaviour of the target system at these specific interpolation points. Therefore, by choosing a set of key input frequencies (from a dynamic perspective) as interpolation points, one of the ideal features, discussed earlier in this section, can be fulfilled straightforwardly. In addition to the choice of the matching frequencies, this method allows the selection of the eigenvalues of the time-domain approximated system; it is thus possible to enforce some essential physical properties of the WEC, such as input-output stability. In this paper, a moment-matching approximation of both the force-to-motion dynamics and the radiation force convolution are presented for the float body of the OPT WEC (see Edwards and Mekhiche (2014) for further details on the OPT device).

### Notation

Standard notation is used through this paper, with some exceptions further detailed in this preliminary section. $\mathbb{R}^+$ ($\mathbb{R}^-$) denotes the set of non-negative (non-positive) real numbers. $\mathbb{C}^0$ denotes the set of pure-imaginary complex numbers and $\mathbb{C}^-$ denotes the set of complex numbers with negative real part. The symbol 0 stands for any zero element, according to the context. The symbol $\mathbb{I}_n$ denotes an order $n$ identity matrix. The spectrum of a matrix $A \in \mathbb{R}^{n\times n}$, i.e. the set of its eigenvalues, is denoted as $\sigma(A)$. The symbol $\bigoplus$ denotes the direct sum of $n$ matrices, i.e. $\bigoplus_{i=1}^{n} A_i = \text{diag}(A_1, A_2, \ldots, A_n)$. The notation $\mathfrak{R}\{z\}$ and $\mathfrak{I}\{z\}$, with $z \in \mathbb{C}$, stands for the *real-part* and the *imaginary-part* operators, respectively. The expression $\|x\|_2$, with $x \in \mathbb{C}^{n\times 1}$, denotes the $\ell^2$-norm of the complex-valued vector $x$. The *Kronecker product* between two matrices $M_1 \in \mathbb{R}^{n\times m}$ and $M_2 \in \mathbb{R}^{p\times q}$ is denoted as $M_1 \otimes M_2 \in \mathbb{R}^{np\times mq}$ while the convolution between two functions $f(t)$ and $g(t)$ over a finite range $[0, t]$, i.e. $\int_0^t f(\tau)g(t-\tau)d\tau$ is denoted as $f * g$. The Fourier transform of a function $f(t) \in L^2(\mathbb{R})$ is denoted by $\mathscr{F}\{f(t)\} \equiv \hat{f}(t)$, where $L^2(\mathbb{R})$ is the function space of all real-valued square-integrable functions. Finally, the symbol $\varepsilon_n \in \mathbb{R}^{n\times 1}$ denotes a vector with odd components equal to 1 and even components equal to 0.
In the remainder of this section, the formal definitions of two important operators are presented, since their definition in the literature can often be ambiguous.

**Definition 1.** (Brewer, 1978) (Kronecker sum) *The Kronecker sum between two matrices $P_1$ and $P_2$, with $P_1 \in \mathbb{R}^{n\times n}$ and $P_2 \in \mathbb{R}^{k\times k}$, is defined (and denoted) as*

$$P_1 \hat{\oplus} P_2 \triangleq P_1 \otimes \mathbb{I}_k + \mathbb{I}_n \otimes P_2. \tag{1}$$

## MODEL ORDER REDUCTION BY MOMENT-MATCHING

Specific notions and definitions of moment-based theory are recalled and summarised in this section. The reader is referred to key studies, such as (Astolfi, 2010) or (Scarciotti and Astolfi, 2017a), where a detailed theoretical development of such concepts is provided.

### Moments for Linear Systems

In this subsection, the notion of *moment* for linear systems, as formulated in (Astolfi, 2010), is presented. Consider a finite-dimensional, single-input, single-output, continuous-time system described, for $t \geq 0$, by the state-space model

$$\dot{x}(t) = Ax(t) + Bu(t), \quad y(t) = Cx(t), \tag{2}$$

where $x(t) \in \mathbb{R}^n$, $u(t) \in \mathbb{R}$, $y(t) \in \mathbb{R}$, $A \in \mathbb{R}^{n\times n}$, $B \in \mathbb{R}^{n\times 1}$ and $C \in \mathbb{R}^{1\times n}$. Consider the associated transfer function

$$W(s) = C(s\mathbb{I}_n - A)^{-1}B \tag{3}$$

and assume that (2) is minimal (i.e controllable and observable).

**Definition 2.** (Antoulas, 2005) *The 0-moment of system* (2) *at $s_i \in \mathbb{C}\backslash\sigma(A)$ is the complex number $\eta_0(s_i) = C(s_i\mathbb{I}_n - A)^{-1}B$. The k-moment of system* (2) *at $s_i \in \mathbb{C}$ is the complex number*

$$\eta_k(s_i) = \frac{(-1)^k}{k!}\left[\frac{d^k}{ds^k}\Big(C(s\mathbb{I}_n - A)^{-1}B\Big)\right]_{s=s_i}, \tag{4}$$

*with $k \geq 1$ integer.*

In (Astolfi, 2010), a new interpretation of moments is given in terms of the steady-state response (provided it exists) of the output of the interconnection between a signal generator and a system (2). This result is recalled, without a proof, in the following theorem (the reader is referred to Astolfi (2010) for a comprehensive proof).

**Theorem 1.** (Astolfi, 2010, Scarciotti and Astolfi, 2017a, Scarciotti and Astolfi, 2017b) *Consider system* (2) *and the signal generator*

$$\dot{\xi}(t) = S\,\xi(t), \quad u(t) = L\xi(t), \tag{5}$$

*with $\xi(t) \in \mathbb{R}^{\nu\times 1}$, $S \in \mathbb{R}^{\nu\times\nu}$, $L \in \mathbb{R}^{1\times\nu}$ and $\xi(0) \in \mathbb{R}^{\nu\times 1}$. Assume that the triple $(L, S, \xi(0))$ is minimal, $\sigma(A) \subset \mathbb{C}^-$, $\sigma(S) \subset \mathbb{C}^0$ and the eigenvalues of $S$ are simple. Let $\Pi \in \mathbb{R}^{n\times\nu}$ be the (unique) solution of the Sylvester equation*

$$A\Pi + BL = \Pi S. \tag{6}$$

*Then there exists a one-to-one relation between the moments $\eta_0(s_1)$, $\eta_0(s_2)$, …, $\eta_0(s_\nu)$, with $s_i \in \sigma(S)$ for all $i = 1, \ldots, \nu$, and the steady-state response $C\Pi\xi$ of the output $y$ of the interconnection of system* (2) *with the signal generator* (5)*. In fact, the moments are uniquely determined by the matrix $C\Pi$.*

As discussed in (Scarciotti and Astolfi, 2017b), the assumption on the eigenvalues of $S$ is a sensible hypothesis, since any contribution from a stable mode will decay exponentially to zero. The minimality of the triple $(L, S, \xi(0))$ implies the observability of $(L, S)$ and the controllability of $(S, \xi(0))$.

**Remark 1.** *From now on, the matrix $C\Pi \equiv \bar{Y}$ is referred as the moment-domain equivalent of $y(t)$.*

Lastly, the following key result is recalled from (Astolfi, 2010, Scarciotti and Astolfi, 2017a).

**Theorem 2.** (Astolfi, 2010, Scarciotti and Astolfi, 2017a) *The family of systems described by*

$$\dot{\Theta}(t) = (S - GL)\,\Theta(t) + Gu(t), \quad \theta(t) = \bar{Y}\,\Theta(t), \tag{7}$$

*parametrised on $G \in \mathbb{R}^{\nu\times 1}$, such as $\sigma(S - GL) \cap \sigma(S) = \emptyset$, contains all the models of dimension $\nu$ interpolating the moments of system* (2) *at $\sigma(S)$.*

**Remark 2.** *The transfer function of the reduced order model* (7) *interpolates the transfer function of system* (2) *at the eigenvalues of $S$. Equivalently, the steady-state output of the reduced order model* (7) *matches exactly the steady-state output of the system resulting from the interconnection between system* (2) *and the signal generator* (5)*.*

**Remark 3.** *The matrix $G$ can be selected to enforce specific properties of the original system on the reduced order model, such as a set of prescribed eigenvalues, as detailed in (Astolfi, 2010, Scarciotti and Astolfi, 2017a) and considered in section "Eigenvalue assignment".*

## WEC EQUATIONS OF MOTION

A 1-DoF (degree of freedom) WEC is considered in this study, since the extension of the algorithm to multiple degrees of freedom can be done in an analogous procedure.

### Time-domain formulation

The linearised equation of motion for a 1-DoF device can be expressed in the time-domain in terms of Newton's second law, obtaining the following linear hydrodynamic formulation:

$$m\ddot{x}(t) = \mathcal{F}_r(t) + \mathcal{F}_h(t) + \mathcal{F}_e(t), \tag{8}$$

where $m$ is the mass of the buoy, $x(t)$ the device excursion, $\mathcal{F}_e(t)$ the wave excitation force, $\mathcal{F}_r(t)$ the radiation force and $\mathcal{F}_h(t)$ the hydrostatic restoring force. The linearised hydrostatic force for a floating body can be written as $\mathcal{F}_h(t) = -s_h x(t)$, where $s_h > 0$ denotes the hydrostatic stiffness. The radiation force $\mathcal{F}_r(t)$ is modelled using linear potential theory and, using the well-known Cummins' equation (Cummins, 1962), is

$$\mathcal{F}_r(t) = -\mu_\infty \ddot{x}(t) - \int_0^{+\infty} k(\tau)\dot{x}(t-\tau)d\tau, \tag{9}$$

where $\mu_\infty = \lim_{\omega\to+\infty} A(\omega)$. $\mu_\infty > 0$ represents the added-mass at infinite frequency, $A(\omega)$ is the radiation added mass and $k(t) \in L^2(\mathbb{R})$ is the (causal) radiation impulse response, containing all the memory effect of the fluid response. Finally, the complete linearised equation of motion of the WEC is given by

$$(m+\mu_\infty)\ddot{x}(t) + k(t) * \dot{x}(t) + s_h x(t) = \mathcal{F}_e(t), \tag{10}$$

The equation of motion (10) is of a Volterra integro-differential form, specifically of the convolution class (Wazwaz, 2011). The internal stability of such an equation, for the WEC case, has been analysed and guaranteed for any physically meaningful values of the parameters and the convolution kernel $k(t)$ involved (Falnes, 2002).

### Frequency-domain formulation

Since the mapping in (10) has a well-defined steady-state response, it is often useful to perform a frequency-domain analysis of such a system. Applying the Fourier transform to (10), and considering velocity as the measurable output, the following representation

$$\hat{\dot{x}}(j\omega) = \mathcal{F}_e(j\omega)H(j\omega), \tag{11}$$

where $H(j\omega)$ represents the force-to-velocity frequency response, holds. $H(j\omega)$ is a function of a specific set of characteristic frequency-dependent parameters, namely

$$H(j\omega) = \frac{1}{B(\omega) + j\omega\left[A(\omega) + m\right] + \dfrac{s_h}{j\omega}}, \tag{12}$$

where $B(\omega)$ is the radiation damping of the device (Falnes, 2002). The hydrodynamic parameters $A(\omega)$ and $B(\omega)$ can be efficiently obtained using existing BEM solvers, such as WAMIT or NEMOH.

### Ogilvie's relations: mapping between time and frequency

(Ogilvie, 1964) established a direct relationship between time-domain (10) and frequency-domain (11) models, as a function of the parameters $B(\omega)$ and $A(\omega)$, and the radiation kernel $k(t)$, using the definition of the Fourier transform, namely

$$\begin{aligned} B(\omega) &= \int_0^{+\infty} k(t)\cos(\omega t)dt, \\ A(\omega) &= \mu_\infty - \frac{1}{\omega}\int_0^{+\infty} k(t)\sin(\omega t)dt. \end{aligned} \tag{13}$$

It follows that the impulse response $k(t)$ can be written as a mapping involving the frequency-dependent parameters as

$$k(t) = \frac{2}{\pi}\int_0^{+\infty} B(\omega)\cos(\omega t)d\omega. \tag{14}$$

Equation (14) allows a frequency-domain analysis of $k(t)$: a direct application of the Fourier transform, yields

$$\hat{k}(j\omega) = B(\omega) + j\omega\left[A(\omega) - \mu_\infty\right] \equiv K(j\omega). \tag{15}$$

## MOMENT-BASED WEC FORMULATION

The equation of motion presented in (10) needs to be re-written in a more suitable structure, since the theory presented in the section "Model order reduction by moment-matching" is based on a state-space representation of the system under analysis. Considering such a fact, the following state-space representation is proposed:

$$\dot{\varphi}(t) = A_\varphi \varphi(t) + B_\varphi \mathfrak{u}(t), \quad y_\varphi(t) = C_\varphi \varphi(t), \tag{16}$$

where $\varphi(t) = [x(t),\ \dot{x}(t)]^\intercal \in \mathbb{R}^{n\times 1}$, with $n = 2$, is the state-vector of the continuous-time model and $y_\varphi(t) = \dot{x}(t) \in \mathbb{R}$ is the output of the system (assuming velocity as measurable output of the device). The function $\mathfrak{u}(t) \in \mathbb{R}$, assumed to be the input of system (16), is defined as

$$\mathfrak{u}(t) = \mathcal{F}_e(t) - k(t) * \dot{x}(t), \tag{17}$$

Under this assumption, the matrices in (16) are given by

$$A_\varphi = \begin{bmatrix} 0 & 1 \\ -\dfrac{s_h}{m+\mu_\infty} & 0 \end{bmatrix},\ B_\varphi = \begin{bmatrix} 0 \\ \dfrac{1}{m+\mu_\infty} \end{bmatrix},\ C_\varphi = \begin{bmatrix} 0 & 1 \end{bmatrix}. \tag{18}$$

Within the moment-based framework, the input $\mathcal{F}_e$ is expressed as a signal generator (5), written in implicit form as

$$\dot{\xi}_e(t) = S\,\xi_e(t), \quad \mathcal{F}_e(t) = L_e\,\xi_e(t), \tag{19}$$

where the dimension of $S$ and $L$ are as in (5), $\xi_e(t) \in \mathbb{R}^{\nu\times 1}$ and, without loss of generality, the initial condition of the signal generator is chosen as $\xi_e(0) = \varepsilon_\nu$. The matrix $S$ can be written in a real block-diagonal form as

$$S = \bigoplus_{p=1}^{f} \begin{bmatrix} 0 & \omega_p \\ -\omega_p & 0 \end{bmatrix}, \tag{20}$$

where $\nu = 2f$, $f \geq 0$ integer. With this selection of matrices, the assumption on the minimality of the triple $(L, S, \xi_e(0))$ holds as long as the pair $(L, S)$ is observable. Also note that each $\omega_p$ represents a desired interpolation point for the model reduction process (see Remark 2). Under this selection of matrices, the moments of system (16), driven by the signal generator (19), can be computed by solving a Sylvester equation (see Theorem 2). The Sylvester equation for the WEC device case can be written as

$$A_\varphi \Pi_\varphi + B_\varphi(L_e - \bar{Z}) = \Pi_\varphi S, \tag{21}$$

where $\Pi_\varphi \in \mathbb{R}^{n\times\nu}$ and $\bar{Z}$ is the moment-domain equivalent of the radiation convolution term. Note that the moment-domain equivalent of the velocity can be simply expressed in terms of the solution of (21), as $\bar{V} = C_\varphi \Pi_\varphi$.

**Proposition 1.** (Faedo et al., 2017b) *The moment-domain equivalent of the convolution integral in* (9) *can be computed as*

$$\bar{Z} = \bar{V}\mathscr{R}, \tag{22}$$

*where $\mathscr{R} \in \mathbb{R}^{\nu\times\nu}$ is a block-diagonal matrix defined by*

$$\mathscr{R} = \bigoplus_{p=1}^{f} \begin{bmatrix} \mathscr{R}_{\omega_p} & -\mathscr{M}_{\omega_p} \\ \mathscr{M}_{\omega_p} & \mathscr{R}_{\omega_p} \end{bmatrix}, \tag{23}$$

*and its entries depend on the added mass $A(\omega)$ and the radiation damping $B(\omega)$ of the device at each specific frequency induced by the eigenvalues of $S$, as*

$$\mathscr{R}_{\omega_p} = B(\omega_p), \quad \mathscr{M}_{\omega_p} = -\omega_p \left[A(\omega_p) - \mu_\infty\right]. \tag{24}$$

With the analytical definition of the moment-domain equivalent of the radiation force convolution term, the following proposition is recalled from (Faedo et al., 2017b), which allows (21) to be solved.

**Proposition 2.** (Faedo et al., 2017b) *The moment-domain equivalent of the output $y_\varphi$ of system* (16) *can be computed as*

$$\bar{V} = L_e \Phi_\varphi^{\mathscr{R}}, \tag{25}$$

*where*

$$\begin{aligned} \Phi_\varphi^{\mathscr{R}} &= \left[\left(\mathbb{I}_\nu + \Phi_\varphi \mathscr{R}^\intercal\right)^{-1} \Phi_\varphi\right]^\intercal, \\ \Phi_\varphi &= (\mathbb{I}_\nu \otimes C_\varphi)\left(S \hat{\oplus} A_\varphi\right)^{-1} (\mathbb{I}_\nu \otimes -B_\varphi), \end{aligned} \tag{26}$$

*with $\Phi_\varphi^{\mathscr{R}} \in \mathbb{R}^{\nu\times\nu}$ and $\Phi_\varphi \in \mathbb{R}^{n\nu\times n\nu}$.*

Proposition 2 shows an explicit analytical expression for the moment-domain equivalent of the output of system (16). Such a result allows the computation of a reduced order model of system (16) using Theorem 2 in a straightforward way. Explicitly:

$$\tilde{\mathcal{H}}_{\sigma(S)} : \begin{cases} \dot{\Theta}_\varphi(t) = (S - G_\varphi L_e)\,\Theta_\varphi(t) + G_\varphi \mathcal{F}_e(t), \\ \theta_\varphi(t) = \bar{V}\,\Theta_\varphi(t), \end{cases} \tag{27}$$

is the family of reduced order models parametrised in $G_\varphi$, interpolating the moments of system (16) at the eigenvalues of $S$, where $\bar{V} = L_e \Phi_\varphi^{\mathscr{R}}$.

**Remark 4.** *The reduced order model* (27) *has dimension $\nu = 2f$, where $f$ is the number of interpolation points (frequencies) selected. This is a consequence of the fact that, for each frequency $\omega_i$, both $\pm j\omega_i$ are chosen as eigenvalues of the real-valued matrix $S$.*

**Remark 5.** *The notation $\tilde{\mathcal{H}}_{\sigma(S)}$ refers to an approximated time-domain model of the force-to-velocity dynamics of the device under analysis, by matching the frequencies selected in $\sigma(S)$.*

## Eigenvalue assignment

As discussed in Remark 3, the additional degree of freedom provided by $G_\varphi$ can be exploited to arbitrarily assign the eigenvalues of the reduced order model (27), i.e. given a set of eigenvalues $\Sigma_\varphi$, one can select $G_\varphi$ such as $\sigma(S - G_\varphi L_e) = \Sigma_\varphi$. In this case, the following procedure is proposed. Define the following transfer function (notation adopted from Remark 5):

$$\tilde{H}_{\sigma(S)}(s) = \bar{V}\left[s\mathbb{I}_\nu - (S - G_\varphi L_e)\right]^{-1} G_\varphi. \tag{28}$$

The frequency-dependent device parameters are calculated using hydrodynamic codes at a finite number of frequencies $\omega_i \in [\omega_l, \omega_u]$, with a frequency step of $\Delta\omega_i$, where $\omega_l$ and $\omega_u$ represents the lower and upper bound of the range, respectively. The chosen frequency range depends explicitly on the application. Define the complex-valued vectors $H_\omega$, $\tilde{H}_\omega$ as,

$$H_\omega = \begin{bmatrix} H(j\omega_l) \\ H(j(\omega_l + \Delta\omega_i)) \\ \vdots \\ H(j\omega_u) \end{bmatrix}, \quad \tilde{H}_\omega = \begin{bmatrix} \tilde{H}_{\sigma(S)}(j\omega_l) \\ \tilde{H}_{\sigma(S)}(j(\omega_l + \Delta\omega_i)) \\ \vdots \\ \tilde{H}_{\sigma(S)}(j\omega_u) \end{bmatrix}. \tag{29}$$

Then, the proposed optimisation procedure, to assign the eigenvalues of the reduced order model $\Sigma_\varphi \subset \mathbb{C}^-$, can be formulated as,

$$\min_{\Sigma_\varphi \subset \mathbb{C}^-} \|H_\omega - \tilde{H}_\omega\|_2^2. \tag{30}$$

## On the radiation force convolution operation

The radiation convolution term in (9) defines a linear time-invariant system completely characterised by the impulse response function $k(t)$, where the input considered is the velocity of the device $\dot{x}(t)$, i.e.

$$y_k(t) = k(t) * \dot{x}(t). \tag{31}$$

A reduced order model obtained by moment-matching can be achieved using the result on the moment-domain equivalent of such a convolution term, provided in Proposition 1, as developed in the following. Assume that the velocity $\dot{x}(t)$ of the WEC can be written as a signal generator in implicit form, in a similar fashion to (19), expressed as a set of linear differential equations given by

$$\dot{\xi}_k(t) = S\,\xi_k(t), \quad \dot{x}(t) = L_k\,\xi_k(t), \tag{32}$$

with $\xi_k(0) = \varepsilon_\nu$ and $L_k$ such that the pair $(L_k, S)$ is observable. Then, recalling Proposition 1, the moment-domain equivalent of the output of (31) can be straightforwardly computed as $\bar{Y}_k = L_k \mathscr{R}$, and a reduced order model of (31) can be obtained by applying Theorem 3. Specifically:

$$\tilde{\mathcal{K}}_{\sigma(S)} : \begin{cases} \dot{\Theta}_k(t) = (S - G_k L_k)\,\Theta_k(t) + G_k \dot{x}(t), \\ \theta_k(t) = \bar{Y}_k\,\Theta_k(t), \end{cases} \tag{33}$$

is the family of reduced order models parametrised in $G_k$, interpolating the moments of system (31) at the eigenvalues of $S$, where $\bar{Y}_k = L_k \mathscr{R}$. Following Equation (28), the transfer function of the reduced order model (31) can be computed as,

$$\tilde{K}_{\sigma(S)}(s) = \bar{Y}_k\left[s\mathbb{I}_\nu - (S - G_k L_k)\right]^{-1} G_k, \tag{34}$$

and the complex-valued vectors $K_\omega$ and $\tilde{K}_\omega$ are defined as in (29), by considering the frequency response of the radiation convolution kernel $K(j\omega)$ (15) (instead of $H(j\omega)$), and the reduced order model transfer function $\tilde{K}_{\sigma(S)}(s)$ (instead of $\tilde{H}_{\sigma(S)}(s)$). Then, the set of desired eigenvalues $\Sigma_k$ of system (33), can be assigned using the same optimisation criterion described in the section "Eigenvalue assignment", namely,

$$\min_{\Sigma_k \subset \mathbb{C}^-} \|K_\omega - \tilde{K}_\omega\|_2^2. \tag{35}$$

## NUMERICAL EXAMPLE

For this case study, the float body of the OPT point absorber WEC has been chosen, which is shown in Fig.1. For the sake of simplicity, it is assumed that the device only moves in heave. The hydrodynamic coefficients, which have been computed using the BEM software NEMOH, are shown in Fig.2. The radiation added-mass and damping of the WEC can be seen in Figs. 2**a** and 2**b** respectively, the radiation kernel frequency response $K(j\omega)$ in Figs. 2**c** and 2**d**, and the force-to-velocity frequency response $H(j\omega)$ in Figs. 2**e** and 2**f**.

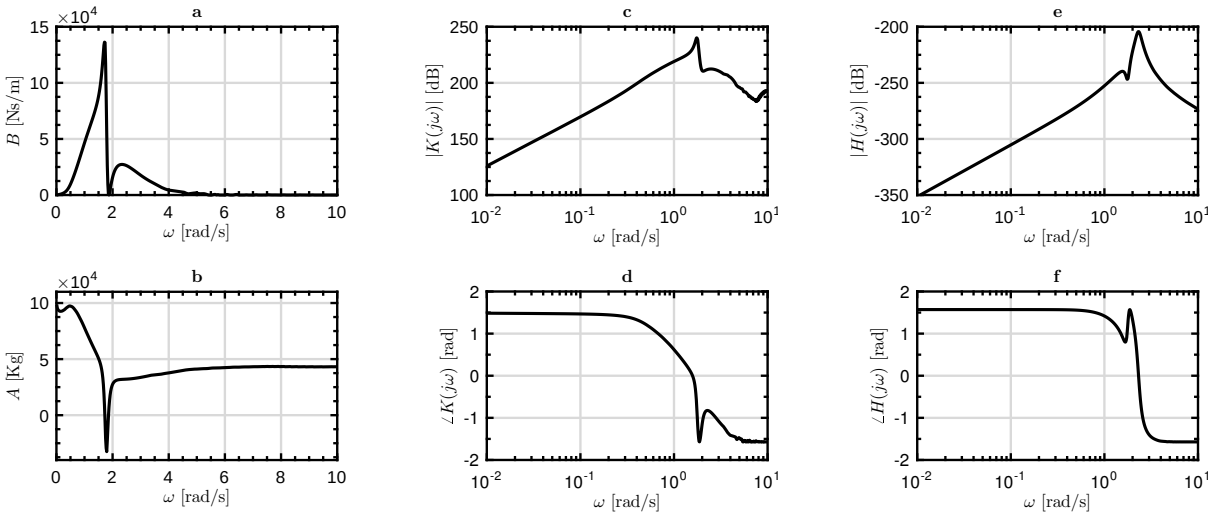


Fig. 2 Device characteristics: **a** radiation damping; **b** radiation added-mass; Bode diagram of the radiation impulse response $K(j\omega)$ (magnitude **c**, phase **d**); Bode diagram of the force-to-velocity frequency response $H(j\omega)$ (magnitude **e**, phase **f**)

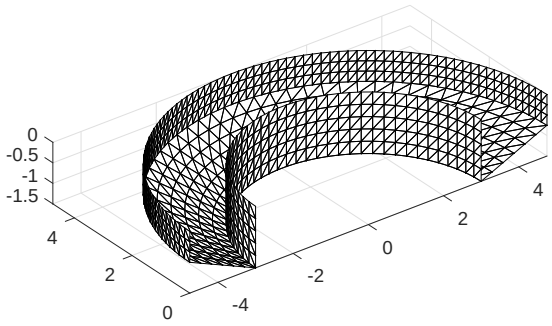

Fig. 1 The low-order mesh for the float of the OPT device

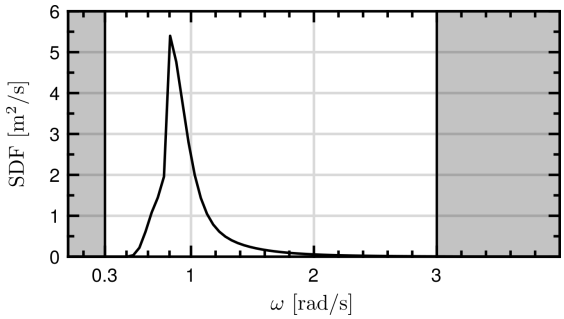


Fig. 3 JONSWAP spectrum considered to generate the irregular waves for this study.

As can be appreciated from Fig.2, the hydrodynamic coefficients have been computed over a frequency range of $\omega = 0.01$ [rad/s] to $\omega = 10$ [rad/s]. However, ocean peak periods are usually between 3 and 16 seconds (Faedo et al., 2017a), which implies that the frequency range of the excitation force, which is the input of the system, lies approximately in the frequency interval $[0.4, 2.1]$ [rad/s]. A more conservative frequency range is considered in this study, specifically $\omega_l = 0.3$ [rad/s] and $\omega_u = 3$ [rad/s].

The numerical examples computed in this section are carried out by considering irregular waves as inputs. Such irregular waves are generated from a JONSWAP spectrum (Hasselman, 1973), with a peak period of $T_\mathrm{p} = 8$ [s], a significant wave height of $H_\mathrm{s} = 2$ [m] and a peak enhancement factor of $\gamma = 3.3$. As shown in Fig.3, all the non-zero values of the spectrum lie in the frequency range selected to approximate the parametric model, which is denoted with a white area in all the following graphs.

## On a force-to-velocity parametric model by moment-matching

In this subsection, the results obtained for the model order reduction of the force-to-velocity frequency response $H(j\omega)$ are discussed. After the frequency range is selected, which is done by inspecting the spectrum of the input depicted in Fig. 3, the first step of this moment-matching based identification technique is to select a set of suitable interpolation points.

Due to the (dynamic) complexity of $H(j\omega)$ for the float of the OPT device, the minimum number of frequencies considered in this study, to achieve moment-matching, is set to two. A sensible choice for a first interpolation point, can be made by inspecting Figs. 2**e** and 2**f**: the resonant frequency of the device represents a key interpolation point, which is approximately $\omega = 2.3$ [rad/s]. In the following, a low frequency component is chosen as the second interpolation point, selected as $\omega = 1$[rad/s]. Fig. 4 shows the frequency response of both the WEC, computed with NEMOH (dashed-black), and the frequency response of the parametric model obtained by applying the moment-matching technique $\tilde{H}_{\{1,2.3\}}(j\omega)$ (solid-red). It can be immediately appreciated that the approximated model matches exactly (up to the numerical imprecision when computing the moments) the target frequency response, at the interpolation points chosen ($\omega = 2.3$ [rad/s] and $\omega = 1$ [rad/s]).

Furthermore, when choosing a third interpolation point, the approximation of $H(j\omega)$ improves significantly, as illustrated in Fig.5.

Fig. 6 shows the time-domain response of the reduced order model $\hat{\mathcal{H}}_{\{1,1.8,2.3\}}$ for irregular waves computed from the spectrum of Fig.3. It can be appreciated that the steady-state behaviour of the approximated model converges to the target steady-state output. For this application case, there is no significant improvement when considering more than three interpolation points in the moment-matching identification framework. However, the approximation error continues to decrease monotonically when the parametric model order increases, as further exemplified in the next subsection.

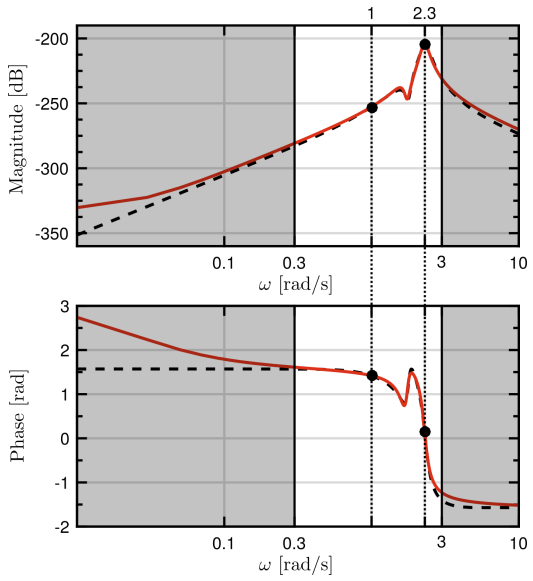


Fig. 4 Bode diagram of the force-to-velocity frequency response computed with the coefficients obtained from NEMOH (dashed-black) and the moment-matching parametric model frequency response (solid-red), for two interpolation points (black dots).

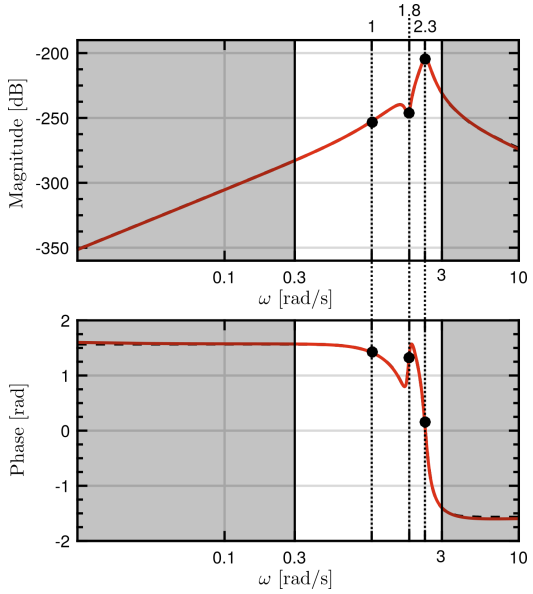


Fig. 5 Bode diagram of the force-to-velocity frequency response computed with the coefficients obtained from NEMOH (dashed-black) and the moment-matching parametric model frequency response (solid-red), for three interpolation points (black dots).

## On a radiation impulse response parametric model by moment-matching

In this subsection, the moment-matching framework to obtain a parametric form of the radiation kernel $K(j\omega)$, as defined in (15), is applied to the dynamics of the studied WEC. Analogously to the force-to-velocity case, there is no significant improvement in the approximation accuracy when selecting more than three interpolation frequencies. As an example, Fig.

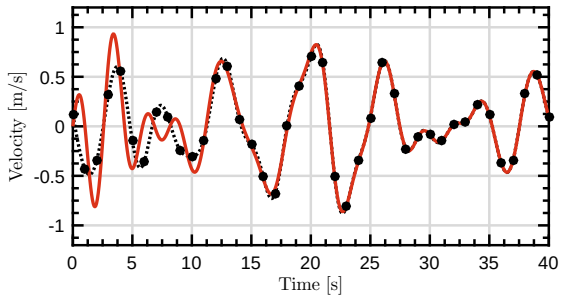


Fig. 6 Comparison between the time-domain output of the reduced order model $\hat{\mathcal{H}}_{\{1,1.8,2.3\}}$ (solid-red) and the force-to-velocity frequency response $\mathcal{H}$ (dotted-black).

7 shows the Bode diagram of the radiation impulse frequency response computed from the hydrodynamic coefficients obtained by NEMOH (dashed-black) and the obtained parametric model frequency response considering three interpolation points $\tilde{K}_{\{0.8,1.75,2.6\}}(j\omega)$ (solid-blue).

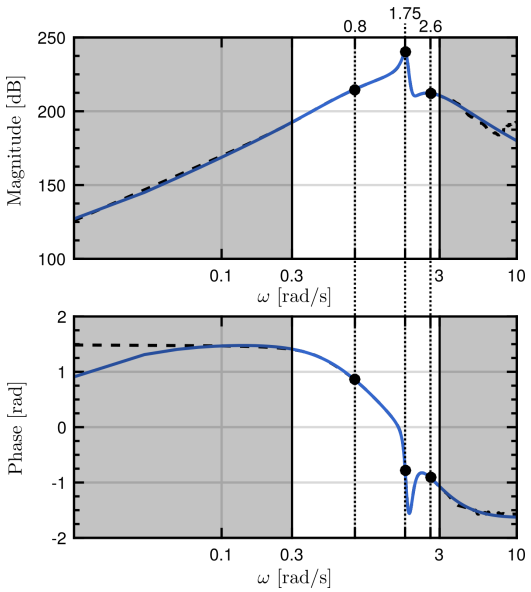


Fig. 7 Bode diagram of the radiation kernel frequency response computed with the coefficients obtained from NEMOH (dashed-black) and the moment-matching parametric model frequency response (solid-blue), for three interpolation points (black dots).

As discussed by Faedo et al. (2017b), the approximated radiation kernel frequency response $\tilde{K}(j\omega)$ should have the same physical properties as the target frequency response $K(j\omega)$ (the reader is referred to Pérez and Fossen (2008) for a comprehensive list of such properties). Among the implication of those physical properties, the transfer function of the device has the following structural characteristics: it has a zero at the origin; it is strictly proper; and is stable. Fig. 8**b** depicts the pole-zero map of the transfer function of the approximated model obtained when considering three interpolation frequencies. It can be acknowledged that such a parametric model accomplishes all the desired properties.

Another important physical property of radiation forces is passivity. Provided that the results obtained from the BEM solver are accurate, $K(j\omega)$ should be passive and so should be $\tilde{K}(j\omega)$. To demonstrate that the models approximated by the moment-matching technique are usually inher-

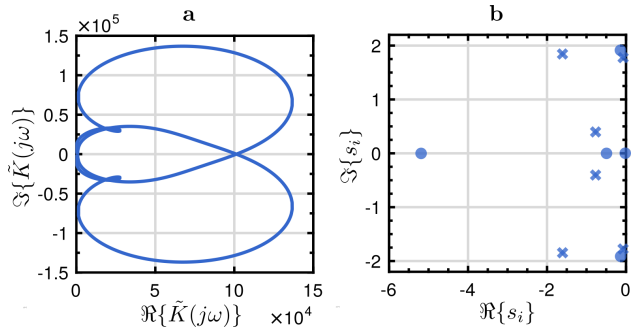


Fig. 8 Pole-zero map of the moment-matching parametric model of the radiation force kernel $\tilde{K}_{\{0.8,1.75,2.6\}}(j\omega)$

ently passive, Fig. 8**a** depicts the Nyquist diagram of $\tilde{K}_{\{0.8,1.75,2.6\}}(j\omega)$. It can be appreciated that the real-part of such an approximated frequency response is always positive and, therefore, the system is passive (the reader is referred to Khalil (1996) for a comprehensive demonstration on the passivity conditions for a linear system). Note that passivity is not explicitly ensured by the moment-matching technique described in this study. However, a nonlinear constraint can be added to the optimisation process defined in (35) to explicitly guarantee passivity, as discussed in (Faedo et al., 2017b).

In Fig. 9, the quality of the time-domain response of the approximated model is further exemplified, showing the radiation impulse response computed using the data obtained from NEMOH (dotted-black), and the impulse response of the reduced order model $\tilde{\mathcal{K}}_{\{0.8,1.75,2.6\}}$.

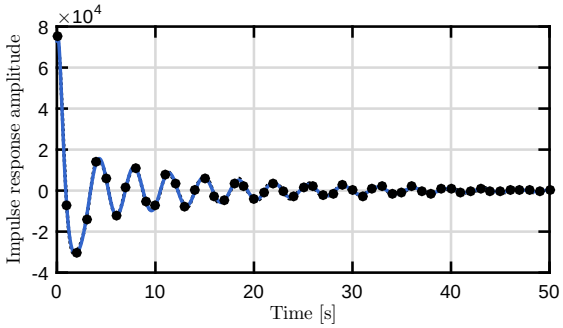


Fig. 9 Comparison between the radiation impulse response computed with data from NEMOH (dotted-black) and the impulse response of $\tilde{\mathcal{K}}_{\{0.8,1.75,2.6\}}$.

Finally, Fig. 10 shows the approximation error of the obtained parametric models of both the force-to-motion and radiation impulse frequency responses for different model orders $\nu$ (i.e. different number of interpolation points). The error is given in terms of the Mean Absolute Percentage Error (MAPE) between the frequency domain data computed using the data from NEMOH $Z_\omega \in \mathbb{C}^{g\times 1}$ and the reduced order model frequency response $\tilde{Z}_\omega \in \mathbb{C}^{g\times 1}$, for the frequency range selected for the approximation[1], i.e.

$$\text{MAPE} = \frac{100}{g}\sum_{i=1}^{g}\left|\frac{Z(j\omega_i)-\tilde{Z}(j\omega_i)}{Z(j\omega_i)}\right|. \tag{36}$$

As previously discussed, the approximation error decreases when the order $\nu$ increases, for both the force-to-motion and the radiation kernel frequency response.

[1]Note that the vectors $Z_\omega$ and $\tilde{Z}_\omega$ are constructed as in (29).

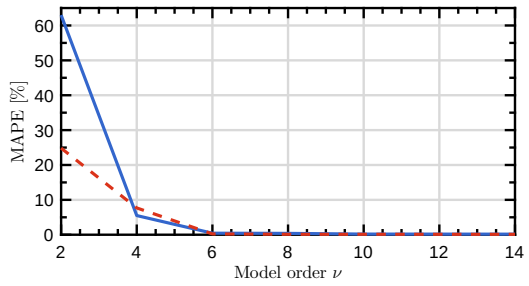


Fig. 10 Error (MAPE) of both the force-to-velocity (dashed-red) and radiation impulse response (solid-blue) approximation models for different orders $\nu$.

## Comparison with existing strategies

In this subsection a comparison between methods proposed in (Pérez and Fossen, 2008) (NTNU), (Duclos et al., 2001, De Prony, 1795) (Prony's) and the moment-matching method considered in this paper, is provided. Such a comparison is given in terms of the Normalised Root Mean Square Error (NRMSE), which is defined as follows:

$$\text{NRMSE} = \sqrt{\frac{\sum\left(\dot{x}(t)-\tilde{\dot{x}}(t)\right)^2}{\sum \dot{x}(t)^2}}, \tag{37}$$

where $\tilde{\dot{x}}(t)$ is the steady-state velocity of the WEC computed using each corresponding approximation model. Since the wave inputs are generated randomly, a mean of 20 different simulations is considered to compute each NRMSE in order to present significant results, as shown in Fig. 11. It is important to notice that, the NTNU and Prony methods (as developed in (Pérez and Fossen, 2008) and (De Prony, 1795), respectively), provide a parametric model of the radiation force convolution term of (10). In the case of the moment-matching strategy presented in this study, both a radiation force convolution term and a force-to-motion parametric model can be obtained.

While, in the case of the force-to-velocity parametric model, the output is directly the velocity of the device, when only the radiation convolution term is approximated, two additional elements in the state-space approximation are required to compute the simulation, i.e. the number of elements in the state vector required to represent the approximation of the convolution term plus two elements to describe the position and the velocity of the device. Therefore, and as can be seen in Fig.11, the methods which approximate the radiation force convolution term have a minimum state-space order of 4.

With the exception of Prony's method, the remaining strategies (NTNU and moment-matching) perform similarly for orders from 8 to 12. It should be noted that, among the methods analysed, only the moment-matching based strategy obtains a monotonically decreasing NRMSE. One can notice that the NRMSE obtained by the NTNU method increases for orders greater than 12. One possible reason for such decline in the accuracy of the approximation could be attributed to the fact that the strategy needs to "flip" any unstable poles to enforce the input-output stability of the parametric model, which translates to a significant error in the phase of the frequency response of such a model. Finally, only the parametric models obtained by the moment-matching method are passive for all the model orders considered. Such results are not extensively discussed in this study due to a lack of space, and the reader is referred to (Faedo et al., 2017b) for further details.

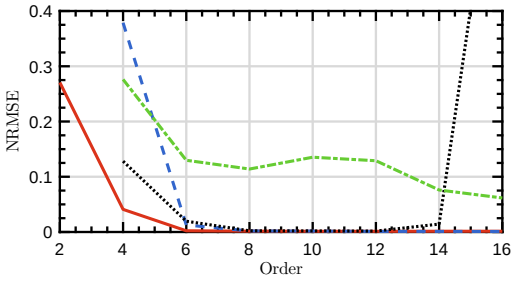


Fig. 11 The NRMSE of the time-domain output computed using a moment-matching force-to-velocity approximated model (solid-red), and using the approximated radiation impulse response computed using moment-matching (dashed-blue), NTNU method (dotted-black) and Prony's method (dash-dot-green) for different model orders.

## CONCLUSIONS

This paper illustrates, via a case study, how to obtain a finite-order parametric model using frequency-domain hydrodynamic data computed by BEMs, for both the force-to-motion and the radiation force convolution operation, based on recent advances on model order reduction by moment-matching. This method matches the steady-state behaviour of the system at a set of selected key frequencies, while enforcing specific physical properties of the studied device, such as input-output stability.
Although the results obtained by the models approximated using this moment-matching framework are similar to those obtained by well-known current methods, this paper shows that the moment-matching strategy is the only method whose approximation error decreases monotonically with an increase of the model order. Additionally, only the approximation of the radiation impulse response computed in the moment-matching framework fulfils all the radiation force physical properties.
Finally, an open-source MATLAB toolbox, to obtain finite-order hydrodynamic models using this moment-matching strategy, is currently under development and it will be available over the next months at the Centre for Ocean Energy Research website[2].

## ACKNOWLEDGMENT

The authors are sincerely grateful to Markel Penalba Retes from the Centre for Ocean Energy Research, for the support and for providing the NEMOH data used to numerically illustrate the proposed strategy. The authors would also like to thank Prof. Alessandro Astolfi and Dr. Giordano Scarciotti from Imperial College London, for useful discussions on the moment-based theory. This material is based upon works supported by Science Foundation Ireland under Grant no. 13/IA/1886.

## REFERENCES

Antoulas, A C (2005). "Approximation of large-scale synamical systems", *SIAM*

Astolfi, A (2010). "Model reduction by moment matching for linear and nonlinear systems", *IEEE Transactions on Automatic Control*, Vol. 55, No 10, pp. 2321–2336.

Babarit, A and Delhommeau, G (2015). "Theoretical and numerical aspects of open source BEM solver NEMOH", *Proc. 11th European Wave and Tidal Energy Conference, Nantes, France*

Brewer, J (1978). "Kronecker products and matrix calculus in system theory", *IEEE Transactions on Circuits and Systems*, Vol. 25, No 9, pp. 772–781.

Cummins, WE (1962). "The impulse response function and ship motions", *Technical report, DTIC Document*

De Prony, G (1795). "Essai éxperimental et analytique: sur les lois de la dilatabilité de fluides élastique et sur celles de la force expansive de la vapeur de lalkool,a différentes températures", *Journal de lécole polytechnique*, Vol 1, No 22, pp. 24–76.

Duclos, G, Clément, A H, Chatry, G, et al (2001). "Absorption of outgoing waves in a numerical wave tank using a self-adaptive boundary condition", *International Journal of Offshore and Polar Engineering*, Vol 11, No 3.

Edwards, K, Mekhiche, M, et al. (2014). "Ocean power technologies powerbuoy®: System-level design, development and validation methodology", *2nd Marine Energy Technology Symposium, METS, Seattle (WA)*.

Faedo, N, Olaya, S, Ringwood, J V (2017a). "Optimal control, MPC and MPC-like algorithms for wave energy systems: An overview", *IFAC Journal of Systems and Control*.

Faedo, N, Peña-Sanchez, Y, Ringwood, J V (2017b). "Finite-order hydrodynamic model determination for wave energy applications using moment-matching", *Submitted to Ocean Engineering*.

Falnes, J (2002). "Ocean waves and oscillating systems: linear interactions including wave-energy extraction", *Cambridge university press*.

Hasselmann, K (1973). "Measurements of wind wave frowth and swell decay during the Joint North Sea Wave Project (JONSWAP)", *Dtsch. Hydrogr. Z.*, Vol 8, pp. 95.

Khalil, H K (1996). "Nonlinear Systems", *Prentice-Hall, New Jersey*.

Newman, J N, Lee, C H (2002). "Boundary-element methods in offshore structure analysis", *Journal of Offshore Mechanics and Arctic Engineering*, Vol 124, No 2, pp. 81–89.

Ogilvie, T F (1964). "Recent progress toward the understanding and prediction of ship motions", *5th Symposium on naval hydrodynamics, Bergen, Norway*, Vol 1, pp. 2–5.

Penalba, M, Kelly, T, Ringwood, J V (2017a). "Using NEMOH for modelling wave energy converters: A comparative study with WAMIT", *Proc. 12th European Wave and Tidal Energy Conference, Cork, Ireland*.

Penalba, M, Touzón, I, Lopex-Mendia, J, Nava, V (2017b). "A numerical study on the hydrodynamic impact of device slenderness and array size in wave energy farms in realistic wave climates", *Ocean Engineering*, Vol 142, pp. 224–232.

Pérez, T, Fossen, T I (2008). "Time-vs. frequency-domain identification of parametric radiation force models for marine structures at zero speed", *Modelling, Identification and Control*, Vol 29, No 1, pp. 1–19.

Scarciotti, G, Astolfi, A (2017a). "Nonlinear model reduction by moment matching", *Foundations and Trends in Systems and Control*, Vol 4, No 3-4, pp. 224–409.

Scarciotti, G, Astolfi, A (2017b). "Data-driven model reduction by moment matching for linear and nonlinear systems", *Automatica*, Vol 79, pp. 340–351.

Wazwaz, A-M (2011). "Volterra integro-differential equations", *Linear and Nonlinear Integral Equations*, pp. 175–212.

[2]http://www.eeng.nuim.ie/coer/